



# Immunophenotyping of Rhesus CMV-Specific CD8 T-Cell Populations

Nicholas L. Pomplun,<sup>1†</sup> Logan Vosler,<sup>1†</sup> Kim L. Weisgrau,<sup>1</sup> Jessica Furlott,<sup>1</sup> Andrea M. Weiler,<sup>1</sup> Hadia M. Abdelaal,<sup>2</sup> David T. Evans,<sup>1</sup> David I. Watkins,<sup>3</sup> Tetsuro Matano,<sup>4</sup> Pamela J. Skinner,<sup>2</sup> Thomas C. Friedrich,<sup>1</sup> Eva G. Rakasz<sup>1\*</sup>

<sup>1</sup>Wisconsin National Primate Research Center, University of Wisconsin-Madison, Madison, Wisconsin

<sup>2</sup>Department of Veterinary and Biomedical Sciences, University of Minnesota, Minneapolis, Minnesota

<sup>3</sup>Department of Pathology, Miller School of Medicine, University of Miami, Miami, Florida

<sup>4</sup>AIDS Research Center, National Institute of Infectious Diseases, Tokyo, Japan

Received 26 February 2020; Revised 12 July 2020; Accepted 20 July 2020

Grant sponsor: National Center for Research Resources, Grant numberP51OD011106

Additional Supporting Information may be found in the online version of this article.

\*Correspondence to: Eva G. Rakasz, PhD, AIDS Vaccine Research Laboratory, 555 Science Dr. Madison, WI 53711  
 Email: erakasz@primate.wisc.edu

<sup>†</sup>These authors contributed equally to this study.

Published online 4 August 2020 in Wiley Online Library (wileyonlinelibrary.com)

DOI: 10.1002/cyto.a.24197

© 2020 The Authors. *Cytometry Part A* published by Wiley Periodicals LLC on behalf of International Society for Advancement of Cytometry.

This is an open access article under the terms of the Creative Commons Attribution-NonCommercial License, which permits use, distribution and reproduction in any medium, provided the original work is properly cited and is not used for commercial purposes.

## • Abstract

A vaccine to ameliorate cytomegalovirus (CMV)-related pathogenicity in transplantation patients is considered a top priority. A therapeutic vaccine must include components that elicit both neutralizing antibodies, and highly effective CD8 T-cell responses. The most important translational model of vaccine development is the captive-bred rhesus macaque (*Macaca mulatta*) of Indian origin. There is a dearth of information on rhesus cytomegalovirus (rhCMV)-specific CD8 T cells due to the absence of well-defined CD8 T-cell epitopes presented by classical MHC-I molecules. In the current study, we defined two CD8 T-cell epitopes restricted by high-frequency Mamu alleles: the Mamu-A1\*002:01 restricted VY9 (VTTLGMALY aa291-299) epitope of protein IE-1, and the Mamu-A1\*008:01 restricted NP8 (NPTDRPIP aa96-103) epitope of protein phosphoprotein 65-2. We developed tetramers and determined the level, phenotype, and functional capability of the two epitope-specific T-cell populations in circulation and various tissues. We demonstrated the value of these tetramers for in situ tetramer staining. Here, we first provided critical reagents and established a flow cytometric staining strategy to study rhCMV-specific T-cell responses in up to 40% of captive-bred rhesus macaques. © 2020 The Authors. *Cytometry Part A* published by Wiley Periodicals LLC on behalf of International Society for Advancement of Cytometry.

## • Key terms

rhesus cytomegalovirus; CD8 T-cell epitope; immunophenotyping; in situ tetramer staining

**AS** a causative agent of considerable morbidity and mortality, human cytomegalovirus (hCMV) has been included among the high priority targets for therapeutic vaccine development since the year 2000 (1-3). hCMV belongs to the Betaherpesvirinae subfamily of Herpesviruses. Having been around for more than 400 million years (4-6), Herpesviruses co-evolved with the immune system of their hosts. As a result, they acquired the ability to establish life-long, productive infection in the presence of abundant cellular and antibody responses. Cytomegaloviruses are highly species-specific pathogens, infecting a wide range of hosts from rodents to primates (7). Primate CMVs are more similar to each other than to CMV in rodents. Cross-species infection is possible, but rare and it mainly occurs between highly related species, such as rhesus and cynomolgus macaques (8, 9). Nonhuman primates represent an invaluable intermediate step in translating vaccination concepts from murine models to humans. Therefore, a thorough understanding of the virus-host interaction between CMVs and nonhuman primates is essential.

Captive-bred rhesus macaques (*Macaca mulatta*) become naturally infected with CMV during the first years of their life. Based on rhCMV-specific IgM and IgG antibody data, seroprevalence can reach up to 100% (10-12). Although the virus is



present in the breast milk, transmission with nursing appears to be less efficient than in human, since seroconversion usually happens well after weaning, mostly following the animals' introduction into the general colony (13). Cellular immune responses can be detected at very low levels as early as six months of age. Circulating T-cell responses are readily detectable in the magnitude of  $10^3$  SFU/million PBMC against viral proteins IE-1, IE-2, or pp65 with IFN- $\gamma$  elispot in adult animals (13). However, in the absence of basic tools, such as rhCMV-specific tetramers, accurate monitoring of these responses cannot be accomplished.

Therefore, our goal in the current study was to define CD8 T-cell epitopes in the viral proteins immediate early protein-1 (IE-1), and phosphoprotein 65-2 (pp65-2). Since tetramers binding to T cells that recognize the human CMV orthologs of these proteins already exist (14, 15), rhCMV-specific tetramers with similar targets will enable the research community to perform direct comparison between the two species.

## MATERIALS AND METHODS

### Animals and Tissue Preparation

We obtained samples from 67, more than three-year old rhesus macaques of Indian origin, housed at the Wisconsin National Primate Research Center (WNPRC). All macaques were cared for in accordance with the guidelines of the Weatherall report and the principles described in the US National Research Council's Guide for the Care and Use of Laboratory Animals, and the US Public Health Service's Policy on Humane Care and Use of Laboratory Animals. The animal welfare assurance no. of WNPRC is A3368-01. The macaques were assigned to various experimental protocols, each approved by the University of Wisconsin Graduate School Animal Care and Use Committee. The animals' MHC-I genotype was determined by the Genetics Services core laboratory of the WNPRC using either sequence-specific PCR analysis or amplicon deep sequencing as described elsewhere (16, 17). Animals were perfused with heparin-containing PBS before tissue harvesting to minimize blood contamination in richly vascularized organs like the lung and kidney. Whole lymph nodes, a 1 cm  $\times$  2 cm portion of the spleen and the salivary gland were cut into 1 mm  $\times$  1 mm pieces in sterile RPMI 1,640 and pressed through a 70  $\mu$ m cell-strainer to remove cellular debris. Strained spleen lymphocytes were purified by Ficoll-Paque PLUS (GE Healthcare Systems, Uppsala, Sweden) density centrifugation. An approximately 1 cm  $\times$  2 cm piece of the lung, the kidney, half of the urinary bladder, and a 5–6 cm-long section of the aorta and the vena cava were cut into small pieces and digested in R10 containing 400 U/ml collagenase Type I, 120 U/ml collagenase Type XI, 60 U/ml hyaluronidase, and 60 U/ml DNase1 at 37°C for one hour, then filtered through a 70  $\mu$ m cell-strainer to remove cellular debris. Cells were counted and further processed for flow cytometry and viral load quantification assays.

### Peptides

15-mers overlapping by 11 amino acids covering the entire length of rhCMV strain 68-1 proteins pp65-2 (18) and IE-1 (19) were synthesized using the services of GenScript Biotech Corp (Piscataway, NJ). GenBank accession numbers are: M93360 for IE-1 (19) and AY186194 for the whole rhCMV 68-1 genome (20). Peptides between 7 and 14 amino acid-long were obtained from the same source and used to define the minimal optimal epitopes. Lyophilized peptides were dissolved in 100% DMSO (Sigma) to create stock solutions of 40 mg/ml concentration. Stock solutions were diluted with sterile HBSS to create 4 mg/ml (100 $\times$ ) working solutions. All stocks were stored at  $-20^\circ\text{C}$ .

### rhCMV Epitope Definition with Elispots

We used freshly isolated or cryo-stored PBMC from EDTA-anticoagulated blood samples in the initial screenings. We detected IFN- $\gamma$  secreting cells using ELISpot PLUS kits (MABTECH Inc, Cincinnati, OH) according to the manufacturer recommendations. We used stimulation conditions and analysis criteria as described previously (21). Briefly,  $1-2.5 \times 10^5$  PBMC/well were stimulated with pools of peptides containing 10 adjacent overlapping 15-mers at approximately 2.2–2.6  $\mu$ M concentration. Wells were imaged and spot-forming cells (SFCs) counted with an AID ELISPOT reader (AID, Strassberg, Germany). Results were considered positive when the mean number of SFCs from duplicate test wells was greater than two times the mean plus two standard deviation of the background SFCs (duplicate wells with no peptide introduced). Positive responses were >50 spots/million cells. Cells stimulated with 10  $\mu$ g/ml Concavalin A (Sigma, Aldrich) were used as positive controls. To determine the phenotype of IFN- $\gamma$  secreting populations we performed ICS using the positive pools as stimulation. The pools were deconvoluted with elispot to identify the stimulating 15-mers, if the responding cells were CD8 positive. 15-mers were serially truncated to unequivocally define the minimal optimal epitope (MOE).

### rhCMV-Specific Primary CD8 T-Cell Lines

We generated rhCMV-specific primary CD8<sup>+</sup> T-cell lines from freshly isolated or cryostored PBMC. Briefly, we incubated  $4-8 \times 10^6$  autologous B-lymphoblastoid cell line (BLCL) with the rhCMV-specific MOE peptide at 20–25  $\mu$ M concentration for 90 min at 37°C, 5% CO<sub>2</sub>. Next, we irradiated the cells with 9000rads and washed them three times to remove any unbound peptide. PBMC was then mixed with the peptide presenting B-LCL at a ratio of 1:1 in RPMI 1640 (GE Healthcare Life Sciences, Pittsburgh, PA) medium supplemented with L-glutamine (GE), antibiotic/antimycotic (GE), and 15% fetal bovine serum (GE) (R15). Recombinant human interleukin-7 (Sigma-Aldrich, St. Louis, MO) was added at 10 ng/ml and the cell mixture was incubated 48 h at 37°C, 5% CO<sub>2</sub>. Cells were then supplemented with R15 containing 100 units/ml recombinant human interleukin-2 (R&D Systems, Minneapolis, MN) (R15-100). Every 2–3 days, the media was refreshed with R15-100. We re-stimulated the

growing cell line with peptide-pulsed B-LCL weekly at a ratio of 1:1. These cells were used to determine MHC-I allele restriction in ICS assays between 4 and 6 weeks after the first stimulation.

### Rhesus Macaque MHC Class I Molecule Transduced Cell Lines

Mamu-A1\*002:01, Mamu-A1\*008:01:01, or Mamu-B\*001:01:02 expressing 721.221 cell lines were generated as described by (22). MHC class I-transduced 721.221 cells were maintained in R10 medium containing 0.5 mg/ml G418. The GenBank accession numbers for rhesus macaque MHC class I sequences are: *Mamu-A1\*002:01* (LN899621), *Mamu-A1\*008:01:01* (LN899628), and *Mamu-B\*001:01:02* (LM608018).

### Tetramer and Surface Phenotype Staining

We pre-incubated  $1 \times 10^6$ – $3 \times 10^6$  cells with APC-conjugated VY9, or NP8 tetramer at 37°C, 5% CO<sub>2</sub> for one hour. (The tetramers were produced by the NIH Tetramer Core Facility at Emory University, Atlanta, GA.) Next, we added the antibodies recognizing the surface phenotypic markers. We used antibodies from BD Biosciences: CCR7 (clone 150503, R&D Systems) FITC, CD3 (clone SP34-2) PE-CF594, CD8 (clone RPA-T8) BV711, CD20 (clone 2H7) Alexa700, CD28 (clone CD28.2,) PE, CD45 (clone D058-1283) BV786; from BioLegend: PD-1 (clone EH12.2H7) BV605; from Beckman Coulter: NKG2a (clone Z199) PE-Cy7, and Near-Infrared Live/Dead Discriminator from Life Technologies. We incubated the cells for 15 min at room temperature, removed any unbound reagents with two washing steps then fixed them with 2% PFA. We acquired the data on a special-order BD LSR II (BD Biosciences, San Jose, CA) equipped with a 50 mW 405 nm violet, a 100 mW 488 nm blue, and a 50 mW 640 nm red laser, 16 detectors, and FACSDiva software version 8.0.1. We collected up to 250,000 events in the lymphocyte gate defined by the forward and side scatter parameters. We analyzed the data using FlowJo version 10.4.2.

### Intracellular Cytokine Staining (ICS)

We incubated up to  $3 \times 10^6$  cells with 2.5 μM peptides or peptide pools in the presence of costimulatory antibodies CD28 (clone L293), CD49d (clone 9F10), and CD107a (clone H4A3) PE antibody, 0.5 μg brefeldin-A and 0.1 nm monensin (BioLegend, San Diego, CA) overnight at 37°C, 5% CO<sub>2</sub>. We used CD3 (clone SP34-2) PE-CF594, and CD8 (clone RPA-T8) BV711 antibodies against surface markers, and Near-Infrared Live/Dead Discriminator to exclude dead cells. After two washing steps we fixed the cells with 2% PFA. We permeabilized the cells with PBS containing 10% FBS, and 0.1% saponin (Millipore-Sigma, St. Louis, MO), and stained them with IFN-γ (clone 4S.B3) FITC, TNF-α (clone Mab11) Alexa700 antibodies for 45 min at room temperature. We obtained each antibody from BD Biosciences. Unbound antibodies were removed with two washing steps. We acquired the data as detailed above. Data analysis was performed using FlowJo version 10.4.2., Pestle 2.0 and Spice 6 (Mario Roederer, Vaccine Research Center, NIH).

### rhCMV Viral Load Quantitation

We isolated DNA from 200 μl fluid samples (plasma, or urine), or  $5 \times 10^6$  cells using the Qiaamp Blood DNA Mini kit (Qiagen, Germantown, MD). We eluted the DNA in 50 μl DEPC water following an additional 5-min incubation at room temperature. We tested the samples for rhCMV by QPCR using the Express QPCR Supermix Universal kit (ThermoFisher Scientific, Waltham, MA) on a LightCycler 96 (Roche, Indianapolis, IN). Cycling conditions were: 95°C for 5 min followed by 50 cycles of 95°C for 15 s, 60°C for 1 min, and 72°C for 1 s. We used primers targeting the rhCMV *UL54* gene (23). The final concentration of each primer was 300 nm. Forward primer – 5'-GATGGGACCGCTCAAGTTTC-3', reverse primer – 5'-TGACGGTAGCGAGGAGACAA-3'.

The final concentration of probe – (6FAM) GGTCGATGGGGTTTTGACTCACGA (BHQ1) was 100 nm. We determined the concentration of the rhCMV DNA in the samples by interpolating onto a standard curve created by tenfold serial dilutions of a fragment of the rhCMV *UL54* gene.

### In Situ Tetramer Staining Combined with Immunohistochemistry

Fresh tissue sectioning, MHC Class I in situ tetramer staining, immunohistochemistry, and confocal imaging was performed as previously described (24, 25). Briefly, we incubated the tissue sections with 0.5 μg/ml FITC-labeled MHC-Class I tetramers overnight at 4°C. For negative control, we used FITC-labeled Mamu-A\*001:01 tetramers loaded with an irrelevant, FLP (FLPSDYFSPV) peptide from the hepatitis B viral core protein. For secondary staining, we incubated the sections with 0.5 μg/ml rabbit-anti-FITC Abs (AbDSerotec, Raleigh, NC), 0.19 μg/ml mouse-anti-human CD20 (clone L26) (Novocastra, Leica Microsystems, Buffalo Grove, IL), and 2 μg/ml rat-anti-human CD3 (clone CD3-12) (ThermoFisher) overnight at 4°C. For tertiary staining, we incubated the sections with 0.3 μg/ml Cy3-conjugated goat-anti-rabbit Abs, 0.75 μg/ml Alexa 488-conjugated goat-anti-rat Abs, and 0.75 μg/ml Cy5-conjugated goat anti-mouse Abs overnight at 4°C. We obtained all three tertiary antibodies from Jackson ImmunoResearch Laboratories (West Grove, PA). We counterstained selected sections with 1 μg/ml DAPI nuclear stain during the tertiary staining. We collected montage images of multiple 512 × 512-pixel z-series using a Leica confocal microscope (step size of 3 μm; starting 5–10 μm from the tissue surface to at least 45 μm deep into each section). B-cell follicles were identified morphologically as clusters of brightly stained, closely aggregated CD20<sup>+</sup> cells, and delineated with Leica software. We used the same software to create montages of multiple projected confocal serial z-scans. Tops and bottoms of tetramer<sup>+</sup> cells at a single Z-scan were distinguished from non-specific staining by stepping up and down through the adjacent z-scans.

### Statistics

For statistical analysis we employed Fisher's exact, or Students' *t* test as indicated, using Microsoft Excel software version 16.16.1 for Macintosh.

## RESULTS

**Definition of rhCMV IE-1 and pp65-2 CD8 T Cell Epitopes**

Initially we screened blood samples from 38 rhesus macaques to find responses elicited by 15-mers of the IE-1 and pp65-2 viral proteins using IFN- $\gamma$  elispot. Among the 13 MHC-I alleles represented in this 38-animal cohort, 3 were shared by at least 2, and 10 were shared by at least eight animals as detailed in Supplementary Table 1. *Mamu-A1\*001:01*, *A1\*002:01*, *A1\*008:01*, *B\*001*, *B\*008*, *B\*017* among others were included in the common alleles. Two responses, shared by multiple animals, were confirmed to be CD8 T-cell responses in subsequent ICS analysis. After deconvoluting the pools, and testing progressively shorter peptides we identified the following minimal optimal epitopes: VY9 - VTTLGMALY (aa291-299) of IE-1 (Fig. 1A), and NP8 - NPTDRPIP (aa96-103) of the viral protein pp65-2 (Fig. 1B). To assure that VY9 and NP8 are truly the minimal optimal epitopes, we performed ICS assays with serial tenfold dilutions of the relevant 9-mer and 8-mer peptides. As the one to two logarithmic lower EC50s of VY9 versus TY8, or NP8 versus HP9 and PP7 show we defined the correct minimal optimal epitopes (Supplementary Fig. 1). Comparative analysis of the MHC-I haplotype of the responding animals enabled us to narrow the presenting alleles to *Mamu-A1\*002:01* for the VY9, and *Mamu-A1\*008:01* for NP8. To support our hypothesis, we screened PBMC samples from additional animals with the minimal optimal epitopes, and found 14 out of 28 *Mamu-A1\*002:01* positive, and 0 out of 10 *Mamu-A1\*002:01* negative animals harboring VY9-specific cells. NP8 elicited response in 24 samples out of 28 *Mamu-A1\*008:01* positive, and 0 of 15 *Mamu-A1\*008:01* negative animals. Since these samples included PBMC from both healthy and SIV-infected animals at the chronic phase of the disease, we analyzed if there was a difference between the frequency, or the magnitude of elispot responses of the two groups. As shown in Supplementary Table 2, the magnitude of average IFN- $\gamma$  response elicited by either the VY9 or NP8 epitope was slightly elevated in the SIV-infected animals, but the differences did not reach significant levels.

To confirm the identity of the restricting MHC-I alleles, we performed ICS assay using VY9 or NP8-specific CD8 T-cell lines and selected Mamu-MHC-I allele expressing transfectants (Fig. 1C,D).

We had VY9, and NP8 tetramers produced, and stained PBMC samples to quantitate cell populations that recognize these epitopes. We discovered the VY9 tetramer to be bound to both CD3<sup>+</sup>CD8<sup>+</sup> and CD3<sup>-</sup>CD8<sup>+</sup> cells in approximately 75% of the *Mamu-A1\*002:01* positive animals (Fig. 2A,B; frequency of tetramer positive CD3<sup>-</sup>CD8<sup>+</sup> cells: median = 3.67%, range 1.41–21.7%,  $n = 18$ , frequency of tetramer positive CD3<sup>+</sup>CD8<sup>+</sup> cells: median = 1.38%, range 0.05–16.55%,  $n = 24$ ). The VY9 tetramer did not bind to cells obtained from *Mamu-A1\*002:01* negative animals (Supplementary Fig. 2). Previous results demonstrated that certain Killer Inhibitory Receptors bind to Mamu-MHC-I molecules

containing the Bw6 motif (26). Therefore, the staining pattern we experienced with the VY9 tetramer was not surprising, in fact it was anticipated. Data showing that the VY9<sup>+</sup>CD3<sup>-</sup>CD8<sup>+</sup> cells were PD-1<sup>-</sup>, expressed the NK cell marker NKG2A/C (Fig. 2C), and could be double stained with the Mamu-A1\*002:01 MHC-I restricted SIVmac239 gag GY9 tetramer further confirmed that the VY9<sup>+</sup>CD3<sup>-</sup>CD8<sup>+</sup> were in fact NK cells (Fig. 2D, E). The NP8 tetramer bound only to T cells in the *Mamu-A1\*008:01* positive animals (data not shown).

**Tissue Distribution, Phenotype and Functional Capability of rhCMV-Specific T Cells**

Analyzing blood samples from a cohort of healthy animals showed, that VY9-specific cells were present at higher frequency (average  $\pm$  SD = 1.41  $\pm$  1.03% of CD8<sup>+</sup> T cells, range = 0.068–3.46%,  $n = 8$ ) than NP8-specific cells in circulation (average  $\pm$  SD = 0.35  $\pm$  0.54% of CD8<sup>+</sup> T cells, range = 0.026–1.92%,  $n = 11$ ; Fig. 3A). The two populations differed significantly in their cellular composition as well: while the overwhelming majority of the VY9-specific cells were of CCR7<sup>-</sup>CD28<sup>-</sup> effector memory phenotype (TEM<sub>2</sub>) (average  $\pm$  SD = 87.99  $\pm$  12.97% of tetramer positive population, range = 60.4–99.3%,  $n = 8$ ), the NP8-specific population contained fewer TEM<sub>2</sub> cells (average  $\pm$  SD = 45.61  $\pm$  28.06% of tetramer positive population, range = 8.22–95.7%,  $n = 11$ ; Fig. 3B). This pp65-2 epitope-specific cell population frequently included a large portion of CD28<sup>+</sup>CCR7<sup>-</sup> TEM1 phenotype (9 of 11 samples contained >30% TEM1 within the tetramer positive population, average  $\pm$  SD = 47.24  $\pm$  23.94% range = 4.17–80.8%), and a minor CD28<sup>+</sup>CCR7<sup>+</sup> central memory population (average  $\pm$  SD = 7.03  $\pm$  5.11% range = 0–17.8%). These significant differences suggest that peptides derived from the early IE-1 protein are presented on many more target cells, than peptides from the late pp65-2 protein.

Cytomegaloviruses have broad cell tropisms. Epithelial cells, fibroblasts, myeloid cells, hematopoietic progenitors, endothelial cells, and B cells are susceptible targets (27–30). Consequently, the presence of rhCMV-specific cells throughout the body is highly predictable. However, immune compartments of different anatomical locations must conform with different physiological demands. The cells' functional adaptation can be traced by phenotypic and functional markers. Therefore, we investigated the distribution of VY9- or NP8-specific CD8<sup>+</sup> T cells in a variety of tissues of four healthy adult animals. Multiple rhCMV DNA positive tissue samples of the animals provided evidence that all four of them were harboring the virus (Supplementary Table 3). In addition to the blood, we included samples from the bone marrow, the axillary, inguinal, and mesenteric lymph nodes and the spleen. CMV has been implicated in vascular diseases (31–33), thus we looked at the aorta and the inferior vena cava. Since the virus is shed in the urine and saliva, we included samples from the kidney, urinary bladder, lung and salivary gland. We investigated the frequency, the differentiation state, and the functional capability of these cells

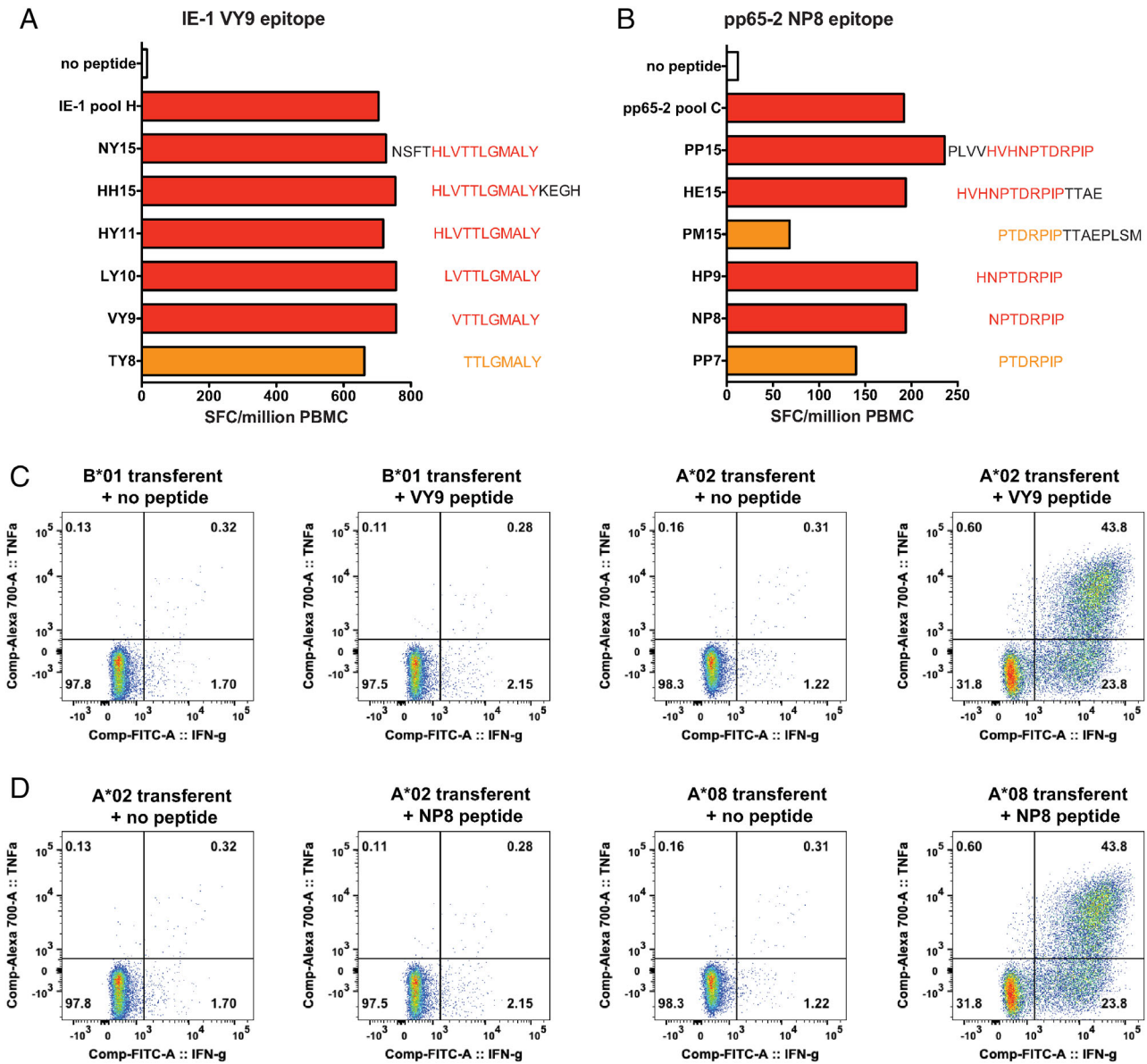


**Fig 1.** Determination of classical MHC-I restricted rhCMV-specific minimal optimal epitopes (MOE). (A) IFN- $\gamma$  elispot data to define the IE-1 VY9 epitope: pool H spanning protein region aa281–aa331. (B) IFN- $\gamma$  elispot data to define the pp65-2 NP8 epitope: pool C spanning protein region aa81–aa131. (C,D) Confirmation of the restricting MHC-I allele with ICS. (C) Coincubation of a primary VY9 epitope-specific CD8<sup>+</sup> T-cell line with Mamu-B\*001:01:02 or Mamu-A1\*002:01 transferents in the absence or presence of VY9 peptide. (D) Coincubation of a primary NP8 epitope-specific CD8<sup>+</sup> T-cell line with Mamu-A1\*002:01 or Mamu-A1\*008:01 transferents in the absence or presence of NP8 peptide. Live, singlet CD8<sup>+</sup> cells were included in the gating strategy.

(Fig. 4A–C). As anticipated, CMV-specific cells were relatively rare (range = 0.0035–0.31% of CD3<sup>+</sup>CD8<sup>+</sup> T cells) in the lymph nodes, and just a small fraction of them reached the terminally differentiated TEM<sub>2</sub> state (CCR7<sup>-</sup>CD28<sup>-</sup>) (range = 4.08–31.8% of tetramer positive T cells). In accordance to their surface phenotype, the majority of them were capable of producing IFN- $\gamma$  and TNF- $\alpha$ , but frequently lacked cytotoxic capability (measured by CD107a expression) (Fig. 4C). Unexpectedly however, rhCMV-specific T cells were enriched in the spleen of three of the four animals (VY9

in r08026 and r07034, NP8 in r13053; range = 0.73–2.72% of CD3<sup>+</sup>CD8<sup>+</sup> T cells). These cells were overwhelmingly of the TEM<sub>2</sub> phenotype (>80% of the tetramer positive cells). Similar enrichment and phenotype were detected at the tertiary immune locations (kidney, urinary bladder, blood vessels, lung, salivary gland, and bone marrow) of the same animals (Fig. 4B). In r08026, VY9-specific CD8 T cells represented unusually high frequencies in the aorta, kidney, and urinary bladder (Fig. 4A, Supplementary Fig. 3). r14073 appeared to be an outlier, since we found no enrichment of the

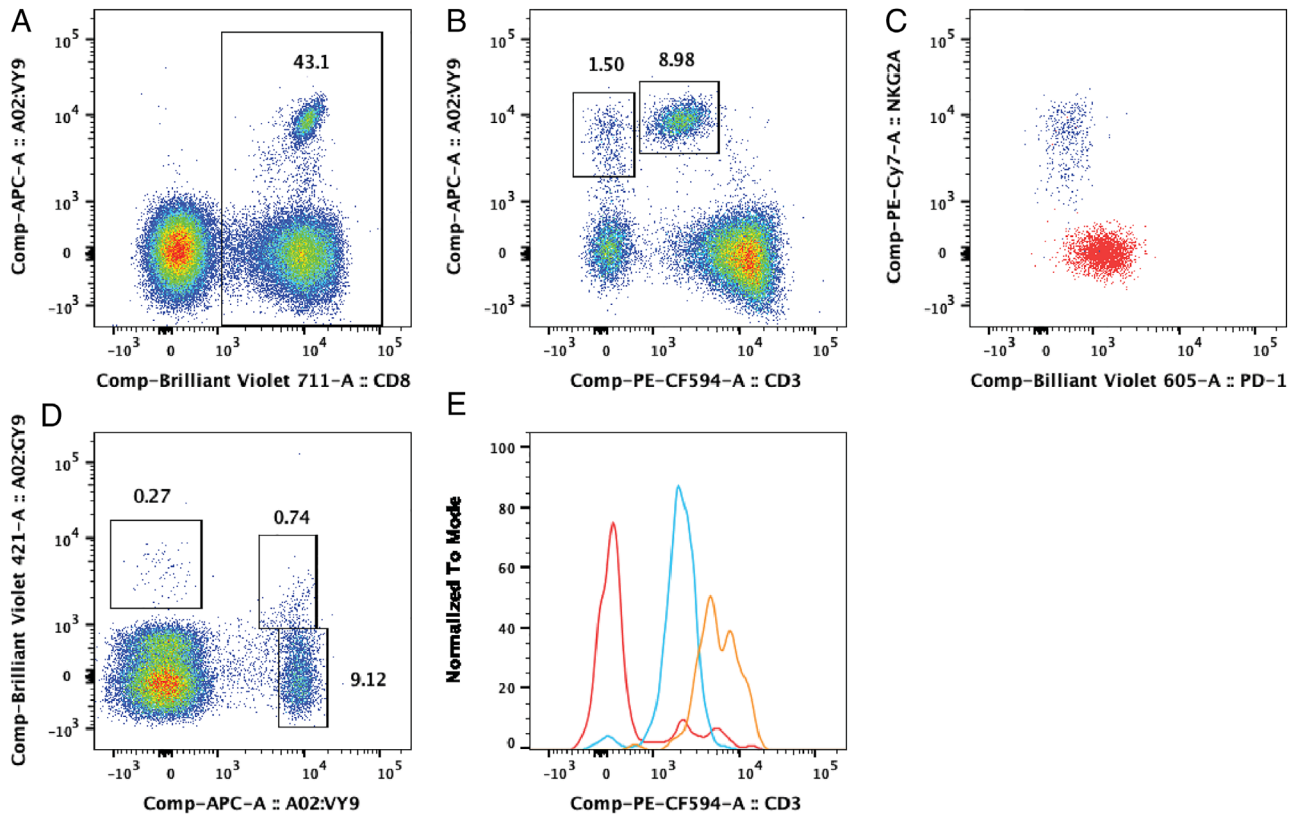


**Fig 2.** Mamu-A1\*002:01 VY9 tetramer binds to both T and NK cells. (A) VY9 staining of live, singlet CD20<sup>-</sup> cells. (B) VY9 staining pattern of the cells gated for CD8 expression. (C) PD-1 and NKG2A/C expression by VY9<sup>+</sup>CD3<sup>+</sup>CD8<sup>+</sup> (blue), and VY9<sup>+</sup>CD3<sup>+</sup>CD8<sup>-</sup> cells (red). (D,E) GY9 and VY9 tetramer co-staining of a PBMC sample from a SIVmac239-infected animal. Live, singlet CD20<sup>-</sup>CD8<sup>+</sup> cells were included in the gating. (E) CD3 antigen expression profile of the tetramer gated populations from panel (D). Red histogram shows the GY9-VY9 double positive population. The blue histogram shows the VY9 single positive population. The orange histogram shows the GY9 single positive population.

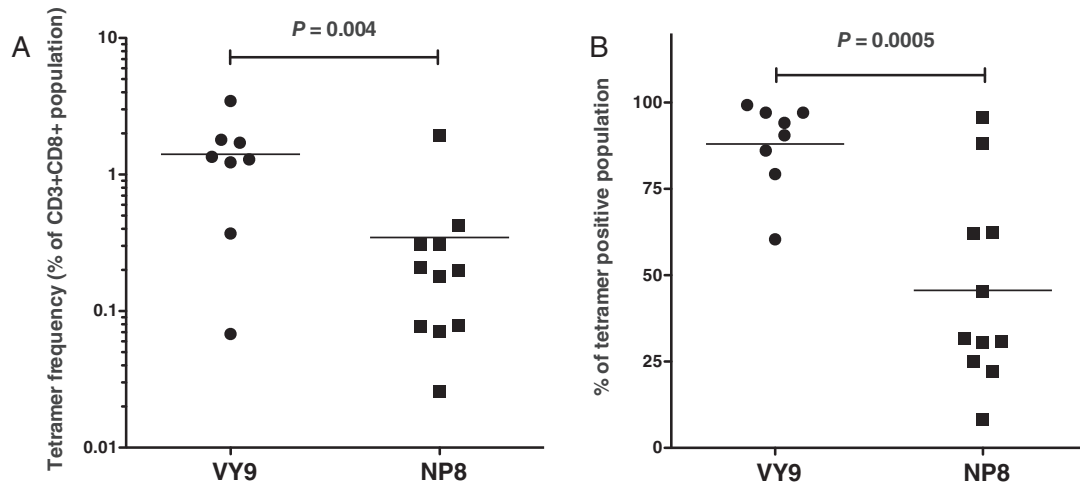


**Fig 3.** Frequency and TEM<sub>2</sub> phenotype expression of the Mamu-A1\*002:01 VY9 and Mamu-A1\*008:01 NP8 cell populations in the peripheral blood. (A) VY9 ( $n = 8$ ) and NP8 ( $n = 11$ ) tetramer frequency in the peripheral blood of healthy rhesus macaques. Live, singlet, CD3<sup>+</sup>CD8<sup>+</sup> tetramer<sup>+</sup> lymphocytes were included in the gating strategy.  $P = 0.0045$  (statistical analysis was performed using Student's  $t$  test, unpaired, one-tailed distribution). (B) TEM<sub>2</sub> cell frequency within the tetramer population of the blood.  $P = 0.0005$  (statistical analysis was performed using Student's  $t$  test, unpaired, one-tailed distribution). Live, singlet, CD3<sup>+</sup>CD8<sup>+</sup> tetramer<sup>+</sup> CCR7<sup>-</sup>CD28<sup>-</sup> lymphocytes were included in the gating strategy.

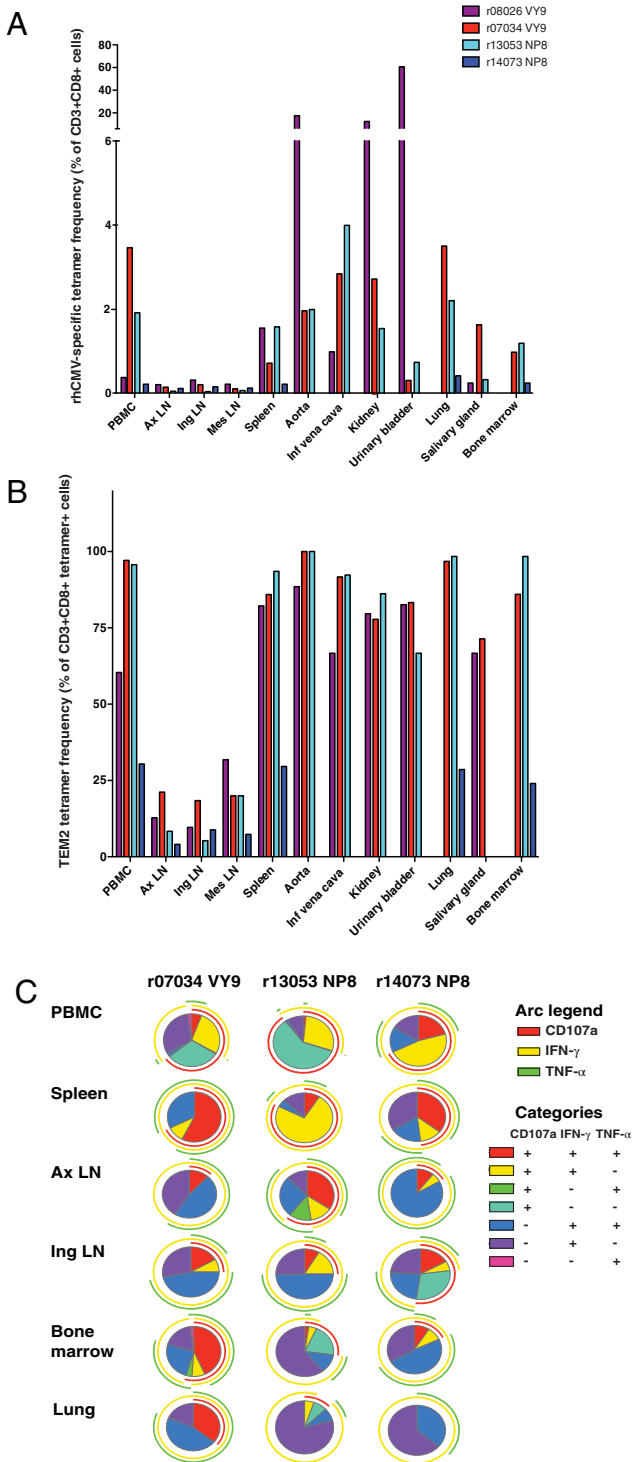


**Fig 4.** Frequency, TEM<sub>2</sub> phenotype expression, and functional capability of the tissue resident Mamu-A1\*002:01 VY9 and Mamu-A1\*008:01 NP8 cell populations. **(A)** Tissue distribution of rhCMV VY9 or NP8-epitope specific T cells. **(B)** Tissue distribution of rhCMV VY9 or NP8-epitope specific T cells with TEM<sub>2</sub> phenotype. **(C)** Functional capabilities of the VY9 and NP8-epitope specific T-cell populations in different anatomic locations of healthy rhesus monkeys. Live, singlet, CD3<sup>+</sup>CD8<sup>+</sup> lymphocytes were included in the gating strategy.

NP8-specific T cells in the tertiary immune sites or the spleen, and only about 30% of the cells possessed TEM<sub>2</sub> phenotype.

Similar differentiation states across various tissues raises the possibility of similar functional phenotypes. Therefore, we analyzed the functional potential of VY9- or NP8-specific T cells in tissues where the number of isolated lymphocytes allowed us to perform intracellular cytokine staining (blood, spleen, lymph nodes, bone marrow, and lung). Interestingly, we could not detect IFN- $\gamma$ , TNF- $\alpha$ , or CD107a response to VY9 peptide stimulation in r08026, in spite of the presence of tetramer positive cells well above the detection limit (e.g., 1.56% of CD3<sup>+</sup>CD8<sup>+</sup> cells in the spleen) (Supplementary Fig. 4). We later found one more among the seven healthy animals tested, where VY9-specific T cells did not secrete IFN- $\gamma$ , TNF- $\alpha$ , or expressed CD107a as a result of stimulation. (We did not observe similar lack of function for NP8-specific cells.) Data from the remaining three animals showed highly variable functional capability. This was true for different samples within the same animal, and for the same type of samples between different animals. In general, however, a higher proportion of the cells in the blood and spleen were cytotoxic, than the ones in the lung, or bone marrow (Fig. 4C).

### In Situ Staining with rhCMV-Specific Tetramers

Defining the localization of virus-specific T cells in different histological areas of the various organs provides critical clues about the control of pathogen proliferation within the host. For example, data from parallel in situ tetramer staining and SIV RNA hybridization provided evidence that the B-cell areas of secondary lymphoid tissues serve as SIV virus reservoirs (34, 35). Therefore, we determined whether our tetramers could be used for in situ tetramer staining assays. We tested multiple spleen samples from the *Mamu-A1\*002:01* positive r07034 and the *Mamu-A1\*008:01* positive r13053 and found excellent staining with both tetramers. The VY9<sup>+</sup> cells were limited to the extrafollicular area, frequently in close contact with B cells (Fig. 5A,B). NP8-specific cells translocated to the B-cell area, although the distribution was not uniform even within the same sample slide. Some follicles harbored abundant number of NP8-specific cells (Fig. 6A,B), others were devoid of them (Fig. 6C,D). We did not detect significant background staining (Fig. 6E,F).

### DISCUSSION

Here, we report the development of new reagents and a staining strategy to study rhCMV-specific CD8 T-cell responses. The *Mamu-A1\*002:01* allele frequency is close to 20% and the *Mamu-A1\*008:01* frequency is approximately 25% of the rhesus macaques in the National Primate Research Centers. Therefore, the tetramers against these two epitopes combined with intracellular cytokine assays allow the research community to study rhCMV-specific responses in more detail in a large portion of the colony animals. This is especially important during chronic viral infection when virus-specific T cells can become exhausted and cease cytokine secretion

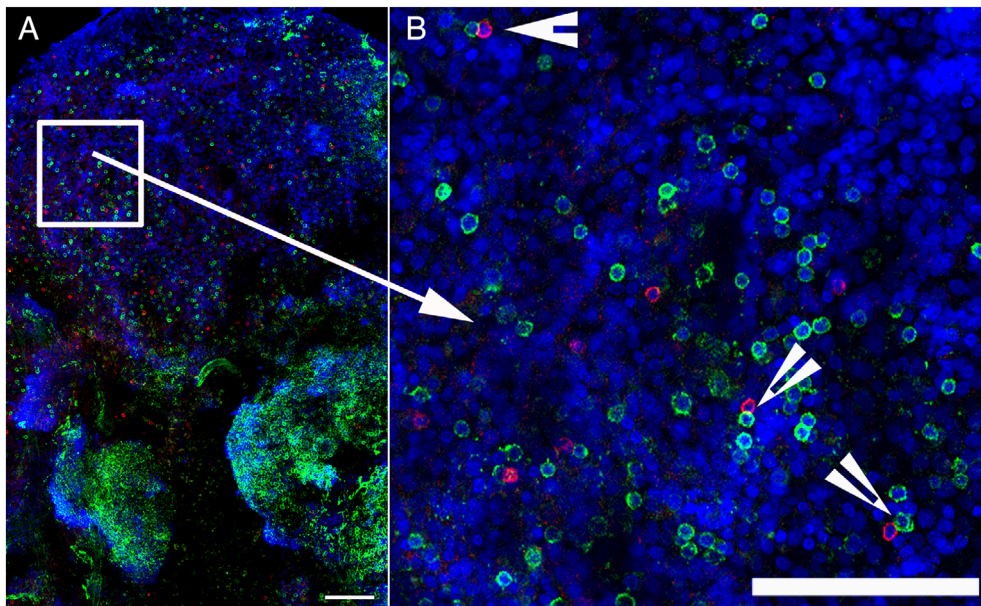


**Fig 5.** Direct contact between rhCMV VY9-specific CTL and B cells in spleen. **(A)** A montage of multiple confocal projected serial z-scans of a sample of animal r07034 (*Mamu A1\*002:01*) stained with Mamu A1\*002:01 VY9 tetramer. **(B)** An enlargement of **(A)** showing direct contact between rhCMV VY9-specific CD8 T cells and B cells within the extrafollicular areas (single confocal z-scan). rhCMV VY9-specific cells: red; CD20<sup>+</sup> B cells: green color; and all nucleated cells stained with DAPI: blue. Direct contact is indicated by white arrowheads. Confocal images were collected using a 20× objective. Scale bars = 100 μm.

(36). Tetramer staining offers the possibility to detect and quantitate these exhausted populations.

We also provided tools to isolate viable rhCMV-specific CD8 T cells by flow cytometry sorting with these new reagents. It is important to emphasize that one of the two tetramers binds to both NK and T cells. While NK cells and CD8 T cells can be distinguished using several surface markers, we found that gating based on the expression of NKG2A/C yielded the most reliable results. NK cells do not express CD3, but rhCMV-specific CD8 T cells frequently downregulated their CD3 level to an extent that separation of the negative and dim population was difficult. For the same reason, the selection of an anti-CD3 antibody conjugated to a bright fluorochrome was essential in the staining panel. Another highly expressed characteristic NK cell marker is CD16 (37). However, this antigen is shed very easily from the cells after a freeze–thaw cycle; therefore, its application as a distinguishing marker on cryostored samples is not appropriate (38, 39). NKG2A/C is expressed at high level on NK cells, and can be expressed at low level on CD8 T cells. Separation of NK cells and CD8 T cells in rhesus macaque samples based on the expression of NKG2A/C is unequivocal.

In the present study, we found that the frequency and memory phenotype of VY9 and NP8 epitope-specific T cells is significantly different in the blood, providing evidence that the individual CMV epitopes are at different stages of a progressive differentiation. These data correspond well both with murine data (40), showing different memory CD8 T-cell phenotypes during chronic MCMV infection, and with the concept of continuous, antigen-driven differentiation of

CMV-specific T cells (41). Additionally, our results correspond to the data from other laboratories, indicating that the magnitude of CMV-specific CD8 T-cell responses tend to be higher against viral proteins that are expressed early in the viral life cycle than the ones expressed later. For example, Sylwester et al. demonstrated that hCMV-specific CD8 T cells against immediate early genes are close to two times more frequent than the ones against late genes (42). Khan et al. provided data showing that the HLA-A\*0201 restricted IE-1 VL9 population is greater than the pp65 NV9 in those adult individuals that possess both responses (43), and Gibson et al. found the same in acutely infected young children (44).

We demonstrated that in addition to blood, lymph nodes, and spleen, a sufficient number of lymphocytes can be isolated from lung, and bone marrow samples to perform both surface phenotype and functional analysis of rhCMV-specific CD8 T cells. It has been established that the functional repertoire of CD8 T cells is influenced by the particular microenvironment where they reside (45). Our data provide an initial glimpse into this compartmentalization. We detected a relative absence of CD107a positive rhCMV-specific cells in the lung and bone marrow, as opposed to the blood and spleen of the same host, where the majority of rhCMV-specific cells possessed this marker. Our results echo the previous findings of Chan et al., showing that the functional capability of circulating rhCMV-specific CD8 T-cell populations is heterogeneous within individual animals and between different epitopes, with a significant fraction possessing cytolytic capacity (46).

We indicated the value of these tetramers in defining the tissue localization of rhCMV-specific cells. Our in situ

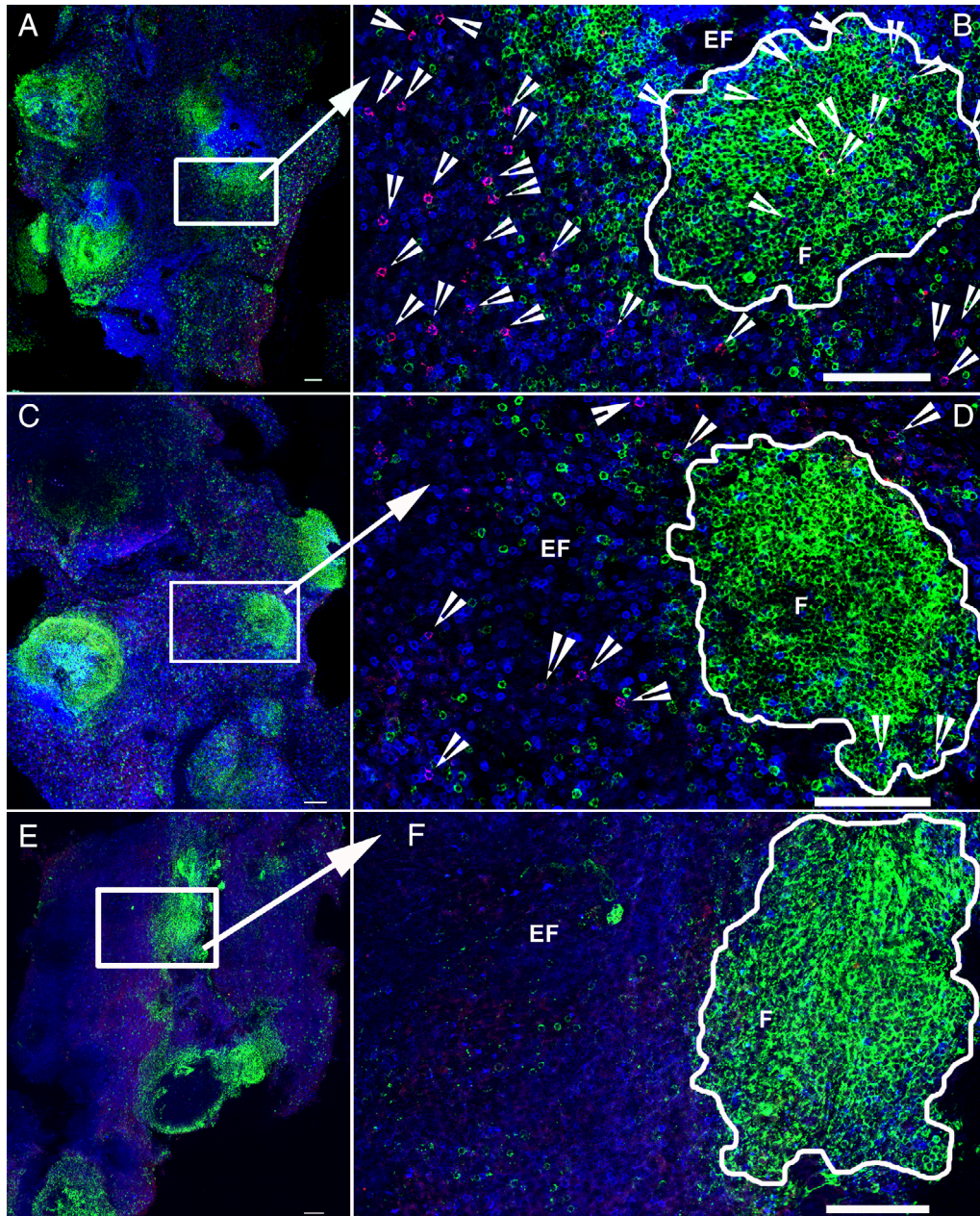


**Fig 6.** Localization of rhCMV NP8-specific cells in the spleen. (A,C) Montages of multiple confocal projected serial z-scans of a sample of animal r13053 (*Mamu-A1\*008:01*<sup>+</sup>) stained with Mamu-A1\*008:01 NP8 tetramer. (B,D) Enlargement from (A) and (C), respectively, showing the range of distribution patterns of rhCMV NP8-specific CTL within follicular (F) and extrafollicular areas (EF) (a single confocal z-scan). (B) Demonstrates a follicle rich with rhCMV NP8-specific CTL that are uniformly distributed within the B-cell follicle. (D) Demonstrates a B-cell follicle with few rhCMV NP8-specific CTL located near the edge of the follicle. rhCMV NP8-specific CTL red, CD3<sup>+</sup> cells blue, and CD20<sup>+</sup> B cells: green color. Tetramer<sup>+</sup> cells are indicated by white arrowheads. Panel (E) (negative control) shows a montage of multiple confocal projected serial z-scans from a spleen tissue section from animal r07034 (*Mamu-A1\*002:01*<sup>+</sup>) rhesus macaques stained with Mamu-A1\*008:01 NP8 tetramers. (F) Enlargement from (E) and shows a single confocal z-scans showing that no rhCMV NP8-specific CTL were detected in the tissue. Confocal images were collected using a 20× objective. Scale bars = 100 μm.

tetramer staining images provided evidence on the close contact between the VY9-specific T cells and CD20<sup>+</sup> B cells within the extrafollicular area. Previously published in vitro data suggested that B cells can be infected with CMV, but the virus is unable to complete its life cycle (47). Whether the

close contact between the VY9-specific T cells and B cells reflects this abortive infection or B cells express this epitope through other mechanism needs to be determined in future studies. The in situ tetramer staining with NP8 tetramer demonstrated that these cells are not evenly distributed within the

numerous follicular areas of the same secondary lymphoid tissue. This technique may provide the tool to understand rhCMV latency in the presence of strong cellular immune responses.

As a summary, here we present for the first time the definition of two new, classical MHC-I restricted rhCMV-specific T-cell epitopes. The reagents developed with these epitopes will advance the efforts aiming to understand CMV-specific cellular responses in one of the most important large animal models of human diseases.

#### ACKNOWLEDGMENTS

We wish to gratefully acknowledge the Scientific Protocol Implementation, the Veterinary Services, and Pathology units, and Genetics Services core laboratory of the Wisconsin National Primate Research Center. We would like to thank Dr. Roger Weisman for his helpful advice and Mr. Jason Weinfurter for his technical support. We acknowledge the NIH Tetramer Core Facility at Emory University for producing the tetramers. This study was supported by National Center for Research Resources grant number P51OD011106 for the Wisconsin National Primate Research Center.

#### AUTHOR CONTRIBUTIONS

**Nicholas Pomplun:** Data curation. **Logan Vosler:** Data curation. **Kimberly Weisgrau:** Data curation. **Jessica Furlott:** Data curation. **Andrea Weiler:** Data curation. **Hadia Abdelaal:** Data curation. **David Evans:** Formal analysis; resources. **David Watkins:** Conceptualization; resources. **Tetsuro Matano:** Resources. **Pamela Skinner:** Formal analysis; resources; supervision. **Thomas Friedrich:** Formal analysis; methodology. **Eva Rakasz:** Conceptualization; formal analysis; project administration; supervision; writing-original draft; writing-review and editing.

#### LITERATURE CITED

- Institute of Medicine (US) Committee to Study Priorities for Vaccine Development. Overview of analytic approach and results. In: Stratton KR, Durch JS, Lawrence RS, editors. *Vaccines for the 21<sup>st</sup> Century: A Tool for Decision Making*. Washington, DC: National Academies Press, 2000; p. 86–89.
- Krause PR, Bialek SR, Boppana SB, Griffiths PD, Laughlin CA, Ljungman P, Mocarski ES, Pass RF, Read JS, Schleiss MR, et al. Priorities for CMV vaccine development. *Vaccine* 2003;32:4–10.
- Nelson CS, Herold BC, Permar SR. A new era in cytomegalovirus vaccinology: Considerations for rational design of next-generation vaccines to prevent congenital cytomegalovirus infection. *NPJ Vaccines* 2018;3:1–9.
- McGeoch DJ, Cook S, Dolan A, Jamieson FE, Telford EA. Molecular phylogeny and evolutionary timescale for the family of mammalian herpesviruses. *J Mol Biol* 1995; 247:443–458.
- McGeoch DJ, Gatherer D. Integrating reptilian herpesviruses into the family of Herpesviridae. *J Virol* 2005;79:725–731.
- McGeoch DJ, Rixon FJ, Davison AJ. Topics in herpesvirus genomics and evolution. *Virus Res* 2006;117:90–104.
- Alford CA, Britt WJ. Cytomegalovirus. In: Roizman B, Whitley RJ, Lopez C, editors. *The Human Herpesviruses*. New York, NY: Raven Press, 1993; p. 227–255.
- Burwitz BJ, Malouli D, Bimber BN, Reed JS, Ventura AB, Hancock MH, Uebelhoer LS, Bhusari A, Hammond KB, Espinosa Trethewy RG, et al. Cross-species rhesus cytomegalovirus infection of cynomolgus macaques. *PLoS Pathog* 2016;12:e1006014. <https://doi.org/10.1371/journal.ppat.1006014>.
- Michaels MG, Jenkins FJ, St George K, Nalesnik MA, Starzl TE, Rinaldo CR. Detection of infectious baboon cytomegalovirus after baboon-to-human liver xenotransplantation. *J Virol* 2001;75:2825–2828.
- Andrade MR, Yee J, Barry P, Spinner A, Roberts JA, Cabello PH, Leite JP, Lerche NW. Prevalence of antibodies to selected viruses in a long-term closed breeding colony of rhesus macaques (*Macaca mulatta*) in Brazil. *Am J Primatol* 2003;59: 123–128.
- Vogel P, Weigler BJ, Kerr H, Hendrickx AG, Barry PA. Seroepidemiologic studies of cytomegalovirus infection in a breeding population of rhesus macaques. *Lab Anim Sci* 1994;44:25–30.
- Swack NS, Hsiung GD. Natural and experimental simian cytomegalovirus infections at a primate center. *J Med Primatol* 1982;11:169–177.
- Kaur A, Itell HL, Ehlinger EP, Varner V, Gantt S, Permar SR. Natural history of postnatal rhesus cytomegalovirus shedding by dams and acquisition by infant rhesus monkeys. *PLoS One* 2018;13:e0206330.
- Zhang D, Shankar P, Xu Z, Hamisch B, Chen G, Lange C, Lee SJ, Valdez H. Tetramer and functional data for pp65: Most antiviral CD8 T cells during chronic viral infection do not express high levels of perforin and are not directly cytotoxic. *Blood* 2003;101:226–235.
- Gordon CL, Miron M, Thome JJC, Matsuoka N, Weiner J, Rak MA, Igarashi S, Granot T, Lerner H, Goodrum F, et al. Tetramer data in human: pp65 and IE-1: Tissue reservoirs of antiviral T cell immunity in persistent human CMV infection. *J Exp Med* 2017;214:651–667.
- Kaizu M, Borchardt GJ, Glidden CE, Fisk DL, Loffredo JT, Watkins DI, Rehauer WM. Molecular typing of major histocompatibility complex class I alleles in the Indian rhesus macaque which restrict SIV CD8 T cell epitopes. *Immunogenetics* 2007;59:693–703.
- Caskey JR, Wiseman RW, Karl JA, Baker DA, Lee T, Maddox RJ, Raveendran M, Harris RA, Hu J, Muzny DM, et al. MHC genotyping from rhesus macaque exome sequences. *Immunogenetics* 2019;71:531–544.
- Yue Y, Kaur A, Zhou SS, Barry PA. Characterization and immunological analysis of the rhesus cytomegalovirus homologue (Rh112) of the human cytomegalovirus UL83 lower matrix phosphoprotein (pp65). *J Gen Virol* 2006;87:777–787.
- Barry PA, Alcendor DJ, Power MD, Kerr H, Luciw PA. Nucleotide sequence and molecular analysis of the rhesus cytomegalovirus immediate-early gene and the UL121–117 open reading frames. *Virology* 1996;215:61–72.
- Hansen SG, Strelow LI, Franchi DC, Anders DG, Wong SW. Complete sequence and genomic analysis of rhesus cytomegalovirus. *J Virol* 2003;77:6620–6636.
- Wilson NA, Keele BF, Reed JS, Piaskowski SM, MacNair CE, Bett AJ, Liang X, Wang F, Thoryk E, Heidecker GJ, et al. Vaccine-induced cellular responses control simian immunodeficiency virus replication after heterologous challenge. *J Virol* 2009;13:6508–6521.
- Banerjee P, Ries M, Janaka SK, Grandea AG III, Wiseman R, O'Connor DH, Golos TG, Evans DT. Diversification of Bw4 specificity and recognition of a non-classical MHC class I molecule implicated in the maternal-fetal tolerance by killer cell Ig-like receptors of the rhesus macaque. *J Immunol* 2018;201:2776–2786.
- Alonso-Guallart P, Duran-Struock R, Zitsman JS, Samenoff S, Pereira M, Stern J, Berglund E, Liore N, Pierre G, Lopes E, et al. Impact of CMV reactivation, treatment approaches and immune reconstitution in a nonmyeloablative tolerance induction protocol in cynomolgus macaques. *Transplantation* 2019;104:270–279. <https://doi.org/10.1097/TP.0000000000002893>.
- Abdelaal HM, Cartwright EK, Skinner PJ. Detection of antigen-specific T cells using in situ MHC tetramer staining. *Int J Mol Sci* 2019;20:5165–5176.
- Li S, Mwakalundwa G, Skinner PJ. In situ MHC-tetramer staining and quantitative analysis to determine the location, abundance and phenotype of antigen-specific CD8 T cells in tissues. *J Vis Exp* 2017;127:1–8.
- Colantonio AD, Bimber B, Niedermeyer WJ, Reeves RK, Alter G, Altfeld M, Johnson RP, Carrington M, O'Connor DH, Evans DT. KIR polymorphism modulate peptide-dependent binding to an MHC class I ligand with a Bw6 motif. *PLoS Pathog* 2011;7:e1001316.
- Lilja AE, Shenk T. Efficient replication of rhesus cytomegalovirus variants in multiple rhesus and human cell types. *Proc Natl Acad Sci USA* 2008;105:19950–19955.
- Yue Y, Kaur A, Lilja AE, Diamond DJ, Walter MR, Barry PA. The susceptibility of primary cultured rhesus macaque kidney epithelial cells to rhesus cytomegalovirus strains. *J Gen Virol* 2016;97:1426–1438.
- Minton EJ, Tysoe C, Sinclair JH, Sissons JG. Human cytomegalovirus infection of the monocyte/macrophage lineage in bone marrow. *J Virol* 1994;68: 4017–4021.
- Mendelson M, Monard S, Sissons P, Sinclair J. Detection of endogenous human cytomegalovirus in CD34+ bone marrow progenitors. *J Gen Virol* 1996;77: 3099–3102.
- Tang-Feldman YJ, Lochhead SR, Lochhead GR, Yu C, George M, Villablanca AC, Pomeroy C. Murine cytomegalovirus (MCMV) infection upregulates P38 MAP kinase in aortas of Apo E KO mice: A molecular mechanism for MCMV-induced acceleration of atherosclerosis. *J Cardiovasc Transl Res* 2013;6:54–64.
- Vliegen I, Duijvestijn A, Grauls G, Herengreen S, Bruggeman C, Stassen F. Cytomegalovirus infection aggravates atherogenesis in apoE knockout mice by both local and systemic immune activation. *Microbes Infect* 2004;6:17–24.
- Ritter JT, Tang-Feldman YJ, Lochhead GR, Estrada M, Lochhead S, Yu C, Ashton-Sager A, Tuteja D, Leutenegger C, Pomeroy C. In vivo characterization of cytokine profiles and viral load during murine cytomegalovirus-induced acute myocarditis. *Cardiovasc Path* 2010;19:83–93.
- Connick E, Folkvord JM, Lind KT, Rakasz EG, Miles B, Wilson NA, Santiago ML, Schmitt K, Stephens EB, Kim HO, et al. Compartmentalization of simian immunodeficiency virus replication within secondary lymphoid tissues of rhesus macaques is linked to disease stage and inversely related to localization of virus-specific CTL. *J Immunol* 2014;193:5613–5625.
- Connick E, Mattila T, Folkvord JM, Schlichtemeier R, Meditz L, Ray MG, McCarter MD, MaWhinney S, Hage A, White C, et al. CTL fail to accumulate at sites of HIV-1 replication in lymphoid tissue. *J Immunol* 2007;178:6975–6983.
- Speiser DE, Utschneider DT, Oberle SG, Münz C, Romero P, Zehn D. T cell differentiation in chronic infection and cancer: Functional adaptation or exhaustion? *Nat Rev Immunol* 2014;14:768–774.

37. Reeves RK, Gillis J, Wong FE, Yu Y, Connoles M, Johnson RP. CD16<sup>+</sup> natural killer cells: Enrichment in mucosal and secondary lymphoid tissues and altered function during chronic SIV infection. *Blood* 2010;115:4439–4446.
38. Currier JR, Eller MA. OMIP-007: Phenotypic analysis of human natural killer cells. *Cytometry* 2012;81:447–449.
39. Pomplun N, Weisgrau K, Evans DT, Rakasz EG. OMIP-028: Activation panel for rhesus macaque NK cell subsets. *Cytometry A* 2015;87:890–893.
40. Munks MW, Cho KS, Pinto AK, Sierro S, Klennerman P, Hill AB. Four distinct pattern of memory CD8<sup>+</sup> T cell response to chronic murine cytomegalovirus infection. *J Immunol* 2006;177:450–458.
41. Pardieck IN, Beyrend G, Redeker A, Arens R. Cytomegalovirus infection and progressive differentiation of effector-memory T cells. *F1000Research* 2018; 1554:1–8.
42. Sylwester AW, Mitchell BL, Edgar JB, Taormina C, Pelte C, Ruchti F, Sleath PR, Grabstein KH, Hosken NA, Kern F, et al. Broadly targeted human cytomegalovirus-specific CD4<sup>+</sup> and CD8<sup>+</sup> T cells dominate the memory compartments of exposed subjects. *J Exp Med* 2005;202:673–685.
43. Khan N, Cobbold M, Keenan R. Comparative analysis of CD8<sup>+</sup> T cell responses against human cytomegalovirus proteins pp65 and immediate early 1 shows similarities in precursor frequency, oligoclonality and phenotype. *J Inf Dis* 2002;185: 1025–1034.
44. Gibson L, Piccinini G, Lilleri D, Revello MG, Wang Z, Markel S, Diamond DJ, Luzuriaga K. Human cytomegalovirus proteins pp65 and immediate early protein 1 are common targets for CD8<sup>+</sup> T cell responses in children with congenital or post-natal human cytomegalovirus infection. *J Immunol* 2004;172:2256–2264.
45. Shane HL, Klonowski KD. Every breath you take: The impact of environment on resident memory CD8<sup>+</sup> T cells in the lung. *Frontiers Immunol* 2014;5:1–10. <https://doi.org/10.3389/fimmu.2014.00320>.
46. Chan KS, Kaur A. Flow cytometric detection of degranulation reveals phenotypic heterogeneity of degranulating CMV-specific CD8<sup>+</sup> T lymphocytes in rhesus macaques. *J Immunol Methods* 2007;325:20–34.
47. Rice GPA, Schrier RD, Oldstone MBA. Cytomegalovirus infects human lymphocytes and monocytes: Virus expression is restricted to immediately-early gene products. *Proc Natl Acad Sci USA* 1984;81:6134–6138.